Further Applications

Peter Harris
Deep Vision Ltd and Sharp Reflections

Time-lapse

Aki & Richards:

$$r_{PP}(\vartheta) \approx \frac{1}{2}\left(\frac{\Delta V_P}{V_P} + \frac{\Delta \rho}{\rho}\right) + \left[\frac{1}{2}\frac{\Delta V_P}{V_P} - 2\frac{V_S^2}{V_P^2}\left(2\frac{\Delta V_S}{V_S} + \frac{\Delta \rho}{\rho}\right)\right]\sin^2\vartheta + \frac{1}{2}\frac{\Delta V_P}{V_P}\left(\tan^2\vartheta - \sin^2\vartheta\right)$$

Empirical or theoretical rock physics relationship between time-lapse changes in pressure, saturation and time-lapse changes in Vp, Vs, density:

$$\frac{\Delta V_p}{V_p} = k_p \Delta S + l_p \Delta P + m_p \Delta P^2$$

$$\frac{\Delta V_s}{V_s} = k_s \Delta S + l_s \Delta P + m_s \Delta P^2$$

$$\frac{\Delta \rho}{\rho} = k_\rho \Delta S$$

k's, *l*'s, *m*'s are empirical constants from core data

AVA inversion using two vintages to get changes in pressure & saturation

Landrø, 2001, Geophysics, 66, No 3

Time-lapse

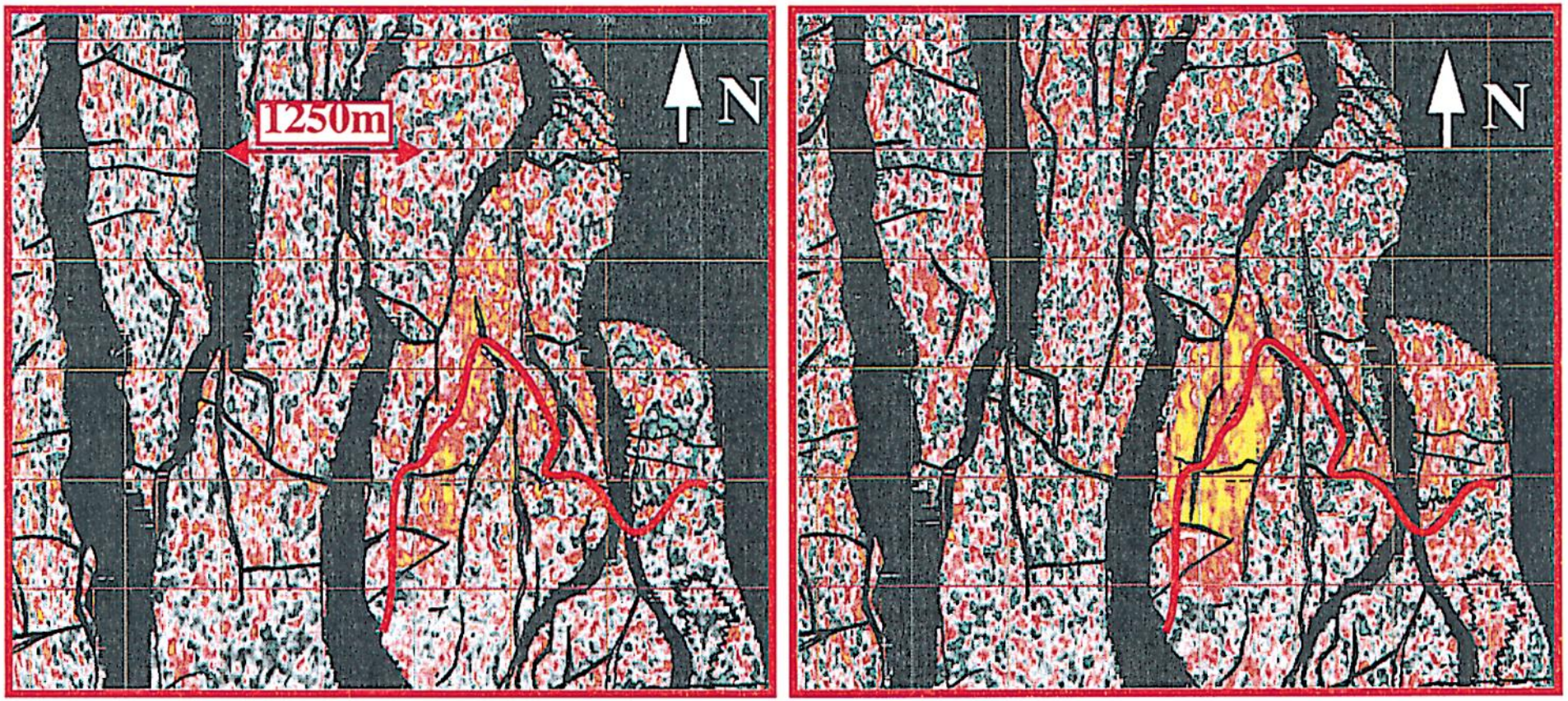

FIG. 11. Comparison of fluid-saturation change attribute map (left) and pore-pressure change attribute map (right) of the top Cook interface. The original oil-water contact is shown in dashed blue lines on both maps. Notice that the pressure anomaly terminates close to faults, while the fluid anomaly terminates close to the original oil-water contact in the western part of this segment.

Landrø, 2001,
Geophysics, 66, No 3

Time-lapse

Further developments using stochastic methods, linking to reservoir simulators

Time-lapse

Many of these methods assume time-lapse changes are linear elasticity: No reservoir compaction, no changes in overburden.

Couple time-lapse inversion to geomechanical modeller (Herwanger)

Attempt to recover components of change in stress tensor (Hawkins, Hatchell)

AVAZ

Anisotropy in fractured or porous rocks is influenced by the local stress field.

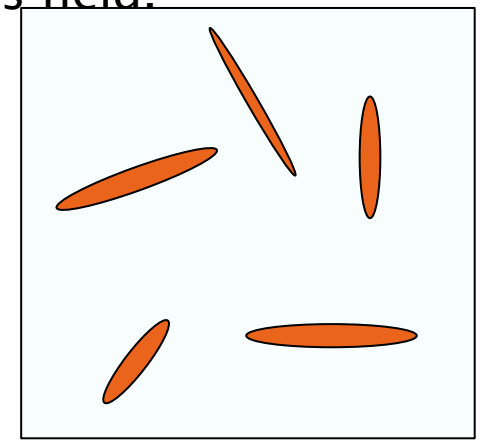

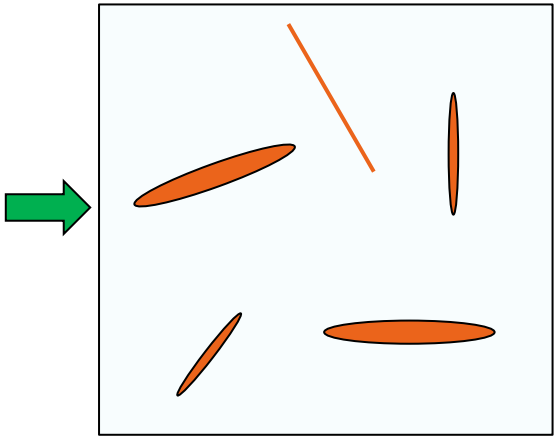

The more compliant cracks close, which introduces a preferred direction in the rock fabric.

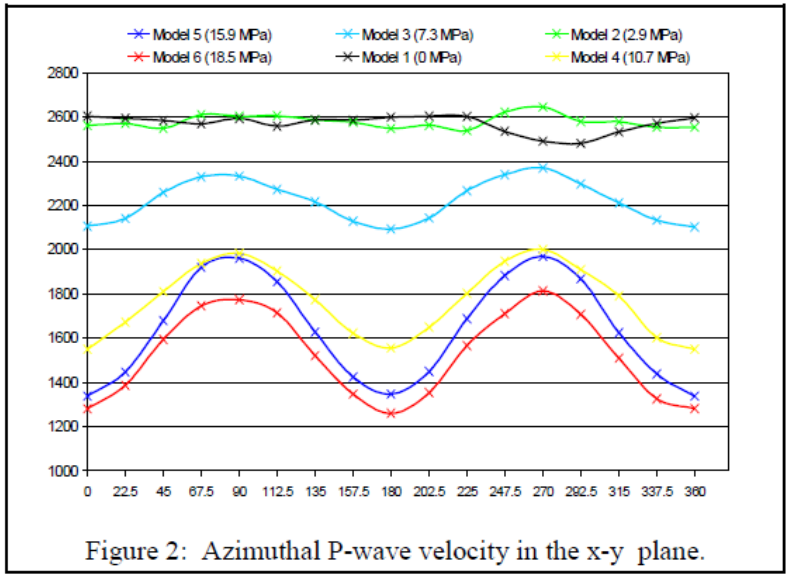

Figure 2: Azimuthal P-wave velocity in the x-y plane.

From Thompson and [illegible] 1999. A study of stress induced anisotropy using the relaxation method on synthetic core.

AVAZ

$$R_{PP}(\vartheta,\varphi) = R_0 + \left(G_{iso} + G_{aniso}\cos^2(\varphi-\varphi_{sym})\right)\sin^2\vartheta + C(\tan^2\vartheta - \sin^2\vartheta)$$

Rüger, 2001

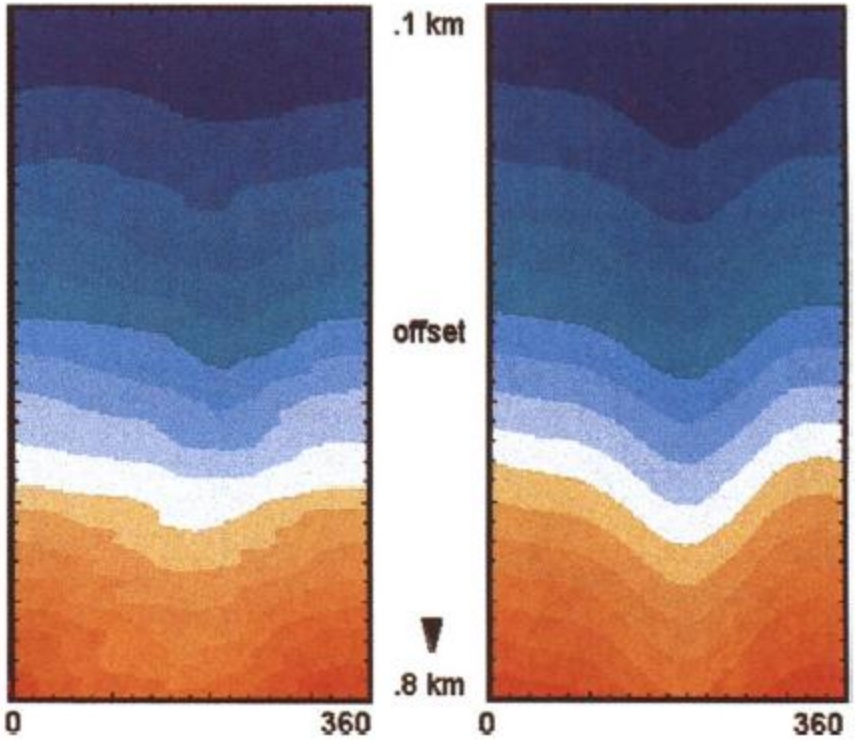

FIG. 7. Base carbonate times versus offset in kilometers (vertical scale) and azimuth in degrees (horizontal scale). Data (left) and the fit to equation (1) (right). The color scale is linear between 0.56 s (blue) and 0.66 s (red).

Leaney, Sayers and Miller, 1999, Analysis of multi-azimuthal VSP data for anisotropy and AVO, Geophysics, 64, 1172-1180

AVAZ

Oriented core measurements

Estimated from AVAZ

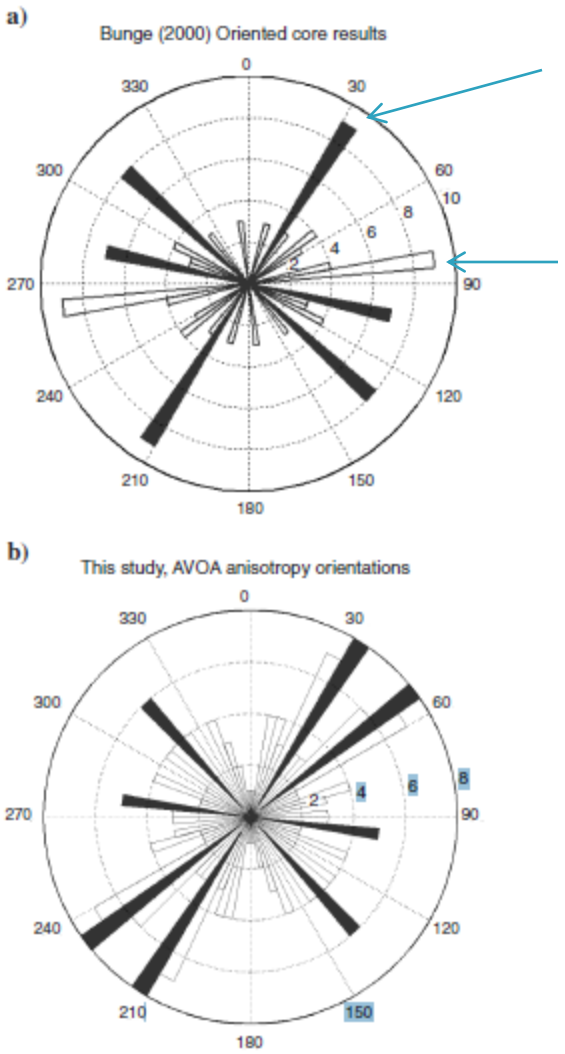

Figure 18. Comparison between (a) Bunge (2000) oriented core fracture orientations and (b) AVOA inversion orientation of anisotropy. Bunge (2000) notes that in (a) open fracture directions are roughly 30°, 315°, and 285°, whereas the healed fracture directions are 80°. AVOA inversion appears to be sensitive to similar open fracture orientations.

Open fractures

Healed fractures

Duxbury et al, Fracture mapping using seismic amplitude variation with offset and azimuth at the Weyburn CO2 storage site, Geophysics, 77, B295-B306

Joint interpretation of seismic and CSEM data

- How to couple the models

Structural constraints. Eg cross-gradient constraint. (Gallardo & Meju, 2004). Assumes that the contours of the different model components are parallel.

Rock physics. Eg Harris et al, 2006, 2009. Assume that underlying lithology controls all physically measurable properties.

Joint inversion

- How to couple the models

Resisivity controlled by porosity, clay content, fluid saturations (Simandoux, Waxman-Smits)

Elastic properties controlled by porosity, clay content, fluid saturations

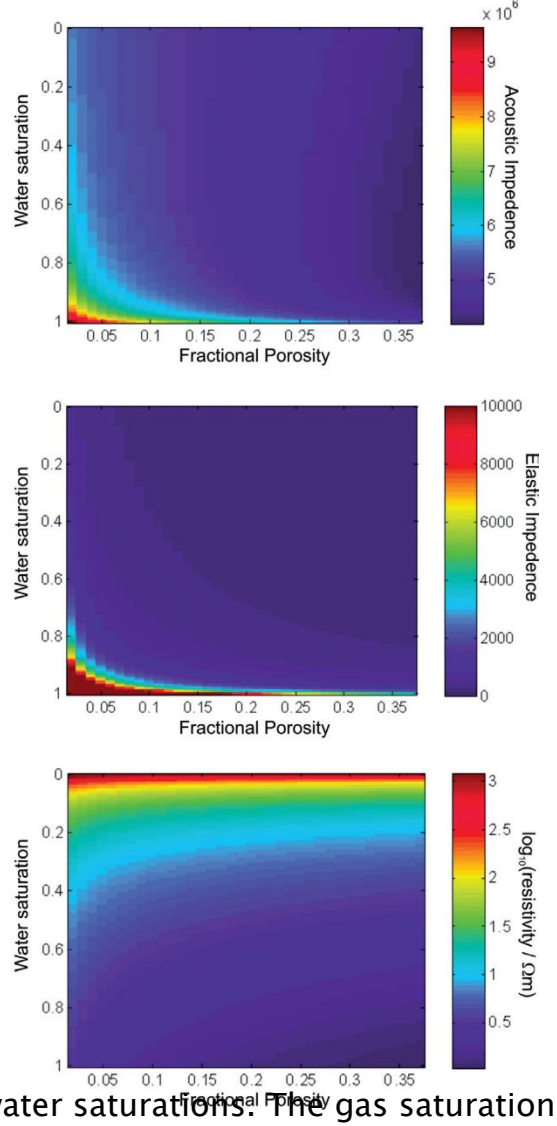

Figure 4
(Top) Acoustic impedance (AI) is plotted for a range of porosities and water saturations. The gas saturation is one minus water saturation. The contours of the AI are more or less vertical in the region of good reservoir (upper right of the plot), showing that AI in this well is largely sensitive to porosity and not at all to gas saturation.
(Middle) Elastic impedance for the same range of porosity and saturation. The surface is rather flat, showing that EI carries little information about either porosity or saturation.
(Bottom) Resistivity for the same models. The contours here are almost horizontal, showing that in this case resistivity is primarily sensitive to saturation rather than porosity.
Harris & MacGregor, 2006

Joint inversion

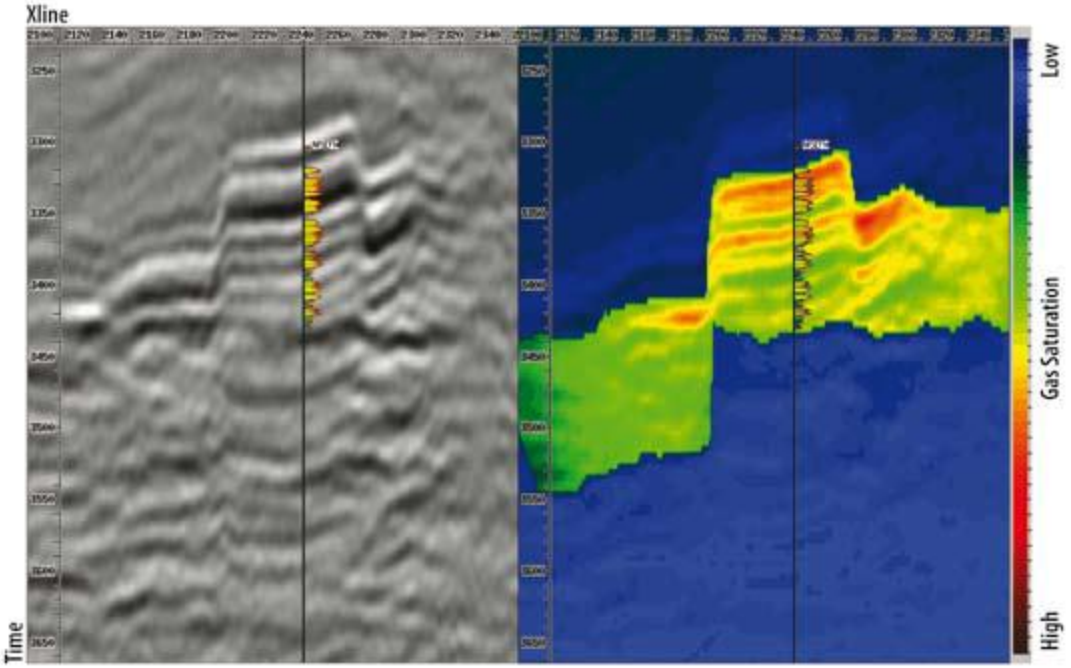

Figure 13 Left, near angle stack of the seismic data, with the gas volume (porosity times gas saturation) log superimposed. Although the seismic image shows the reservoir structure in some detail, it does not, by itself, provide information on the fluid content. Right, gas volume section derived from the combined CSEM and seismic inversions. The low saturation shales stand out clearly as the darker green events within the reservoir unit. The highest gas volume lies at the top of the reservoir, as expected.
Harris et al, 2009